Journal of Computational Physics 321 (2016) 698–707

Contents lists available at ScienceDirect

Journal of Computational Physics

www.elsevier.com/locate/jcp

Higher-order brick-tetrahedron hybrid method for Maxwell's equations in time domain

Johan Winges, Thomas Rylander *

Department of Signals and Systems, Chalmers University of Technology, SE-41296 Göteborg, Sweden

ARTICLE INFO

Article history:
Received 9 September 2015
Received in revised form 8 April 2016
Accepted 31 May 2016
Available online 3 June 2016

Keywords:
Finite element method
Nitsche's method
Higher-order method
Brick-tetrahedron hybridization
Explicit–implicit time-stepping
Maxwell's equations

ABSTRACT

We present a higher-order brick-tetrahedron hybrid method for Maxwell's equations in time domain. Brick-shaped elements are used for large homogeneous parts of the computational domain, where we exploit mass-lumping and explicit time-stepping. In regions with complex geometry, we use an unstructured mesh of tetrahedrons that share an interface with the brick-shaped elements and, at the interface, tangential continuity of the electric field is imposed in the weak sense by means of Nitsche's method. Implicit time-stepping is used for the tetrahedrons together with the interface. For cavity resonators, the hybrid method reproduces the lowest non-zero eigenvalues with correct multiplicity and, for geometries without field singularities from sharp corners or edges, the numerical eigenvalues converge towards the analytical result with an error that is approximately proportional to h^{2p}, where h is the cell size and p is the polynomial order of the elements. For a rectangular waveguide, a layer of tetrahedrons embedded in a grid of brick-shaped elements yields a low reflection coefficient that scales approximately as h^{2p}. Finally, we demonstrate hybrid time-stepping for a lossless closed cavity resonator, where the time-domain response is computed for 300,000 time steps without any signs of instabilities.

1. Introduction

The finite-difference time-domain (FDTD) scheme [1,2] is a very popular numerical algorithm for solving the transient Maxwell's equations. The FDTD scheme is typically formulated on Cartesian grids with explicit time-stepping, which makes it rather efficient and relatively simple to understand and program. However, it suffers from some major drawbacks: (i) the staircase approximation associated with curved and oblique boundaries; (ii) numerical dispersion errors that make it unsuitable for problems that are electrically large; and (iii) difficulties in resolving small geometrical features and rapid field variations. Higher-order finite-difference approximations [3] make it possible to reduce the numerical dispersion errors but they do not solve the problems associated with the staircase approximation and the representation of small geometrical details.

The finite element method (FEM) [4,5] offers a variety of accurate and efficient possibilities for the numerical simulation of electromagnetic problems: (i) it can be operated efficiently on Cartesian grids and it is possible to apply mass-lumping for brick-shaped elements in order to get an explicit time-stepping algorithm [6,7]; (ii) higher-order polynomial approximations of the field solution reduce the numerical dispersion errors; (iii) the FEM allows for unstructured meshes of tetrahedrons

* Corresponding author.
E-mail address: rylander@chalmers.se (T. Rylander).

http://dx.doi.org/10.1016/j.jcp.2016.05.063

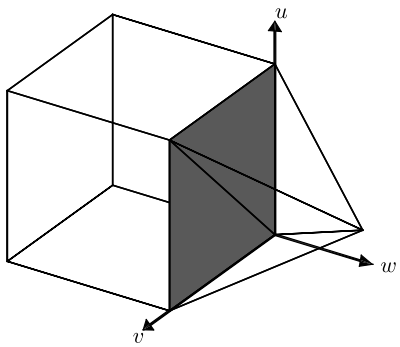

Fig. 1. Geometry of a part of the hybrid interface shown by the two dark gray triangles. The hybrid interface is located in the plane $w = 0$ and it is shared by one brick-shaped element and two tetrahedrons.

that are suitable for local mesh refinement and representation of complex geometry. In terms of the second-order wave equation for the electric field, the conventional FEM exploits a curl-conforming representation for the electric field. For the lowest-order approximation based on so-called edge elements, a structured grid of brick-shaped elements can be connected to unstructured tetrahedrons by means of a layer of pyramids [8], which provides a curl-conforming electric field in the entire computational domain with explicit time-stepping for the brick-shaped elements and implicit (and unconditionally stable) time-stepping for the remaining elements. However, the edge elements on pyramids are not polynomial, which complicates programming and error analysis. In addition, it is inconvenient to deal with mesh generation that involves pyramids. For the lowest-order edge elements, another option is to connect the tetrahedrons directly to the brick-shaped elements in the strong sense [9]. This construction yields an interface with a discontinuous tangential electric field and, despite this characteristic attribute, it displays all the important and attractive properties that such a hybrid method should feature: (i) no spurious solutions; (ii) quadratic convergence for regular problems; (iii) low reflection-coefficient at the hybrid interface; and (iv) stable hybrid explicit–implicit time-stepping given that a Courant condition associated with the explicit elements is fulfilled.

Clearly, it is desirable to construct higher-order versions of this hybrid method. One option is to use a complete-order basis for the tetrahedrons that can be fitted exactly to the incomplete-order basis that is used on the brick-shaped elements. This can be achieved by enforcing pointwise tangential continuity in the strong sense by (i) the projection of the basis of the brick-shaped elements onto the tetrahedral degrees of freedom [10] or (ii) fitting by Galerkin's method such that the tangential field is continuous [11,12]. In comparison with the incomplete-order basis on tetrahedrons, the corresponding complete-order basis contains additional gradient fields that do not contribute to the modeling of the curl of the field and, therefore, hybrid methods that feature a complete-order basis for the tetrahedrons contain degrees of freedom that could be removed.

In this article, we exploit Nitsche's method [9,13,14] to enforce tangential continuity in the weak sense at the hybrid interface between the tetrahedrons and the brick-shaped elements, where the weak form features a stabilization parameter that can be chosen. As a consequence, we can equip both the tetrahedrons and the brick-shaped elements with an incomplete-order basis that has the same type of approximation capabilities and, thus, reduce the degrees of freedom needed for the unstructured tetrahedrons. This is particularly important since a large part of the memory requirements is associated with the matrices that represent Maxwell's equations on the unstructured mesh. (On the structured grid of brick-shaped elements, it is more attractive to use a matrix-free representation of Maxwell's equations [3] and, consequently, only store the field solution in memory.) In addition, our hybrid method can handle a complete-order basis on the tetrahedrons, should it be desirable for the approximation of gradient fields that may be present locally in the vicinity of sharp edges and corners. We exploit a hybrid explicit–implicit time-stepping algorithm with a global time-step that is limited by a Courant condition associated with the explicit time-stepping of the brick-shaped elements. By means of a set of numerical test cases, we demonstrate that our hybrid method is free from spurious solutions and reproduces the correct spectrum for cavity resonators, where the numerical eigenvalues tend towards the exact answer with the expected order of convergence. Given a lossless closed cavity resonator, we also demonstrate hybrid explicit–implicit time-stepping for 300,000 time-steps and note that the solution shows no signs of instabilities. In addition, the hybrid interface yields a low reflection coefficient.

2. Hybrid method

The computational domain Ω is discretized by tetrahedral elements in regions with complex geometrical details, or where local mesh refinement is necessary, and with brick-shaped elements in the homogeneous parts of the computational domain. The region with tetrahedrons is denoted Ω^{tet}, the region with brick-shaped elements is denoted Ω^{bse} and the interface $\Gamma = \partial\Omega^{\text{tet}} \cap \partial\Omega^{\text{bse}}$ connects the two regions with different types of elements. As shown in Fig. 1, each rectangular face of a brick-shaped element that coincides with the interface is connected to two tetrahedral elements, such that the edges of the tetrahedral elements coincide with the edges and the diagonal of the rectangular face.

2.1. Continuum formulation

For time-domain problems, it is natural to use Faraday's law and Ampère's law as a system of first-order differential equations to compute the electric and magnetic field, which is the form exploited in the FDTD scheme [1,15] and similar constructions for higher-order approximations [3]. To formulate the hybrid method presented in this article, it is more convenient to eliminate the magnetic field in order to arrive at a second-order differential equation for the electric field. In frequency domain, we then seek the electric field $\boldsymbol{E}(\boldsymbol{r},\omega)$ that satisfies

$$\nabla\times\nabla\times\boldsymbol{E}-\mu_0\epsilon\omega^2\boldsymbol{E}=\boldsymbol{0} \qquad \text{in } \Omega \tag{1}$$

$$\hat{\boldsymbol{n}}\times\boldsymbol{E}=\boldsymbol{0} \qquad \text{on } \partial\Omega \tag{2}$$

$$\hat{\boldsymbol{n}}\times[\![\boldsymbol{E}]\!]=\boldsymbol{0} \qquad \text{on } \Gamma \tag{3}$$

$$\hat{\boldsymbol{n}}\times[\![\nabla\times\boldsymbol{E}]\!]=\boldsymbol{0} \qquad \text{on } \Gamma \tag{4}$$

where $\hat{\boldsymbol{n}}$ is the unit normal vector at Γ that points away from Ω^{bse}. Here, $[\![\boldsymbol{E}]\!]=\boldsymbol{E}^{\text{bse}}-\boldsymbol{E}^{\text{tet}}$ is the jump of $\boldsymbol{E}$ at the interface Γ. For simplicity, we use the boundary condition (2) for a perfect electric conductor on the outer boundary $\partial\Omega$ of the computational domain Ω. For open-region problems, the boundary condition (2) can be replaced by an appropriate Robin boundary condition.

2.2. Finite element formulation based on Nitsche's method

We expand the electric field in curl-conforming basis functions [5] and use Galerkin's method to derive a finite element method. The tangential component of the electric field may be discontinuous at the interface Γ and, thus, we exploit Nitsche's method [13] to derive the weak formulation

$$\begin{aligned}&\left(\nabla\times\boldsymbol{N}_i^{\text{tet}},\nabla\times\boldsymbol{E}^{\text{tet}}\right)_{\Omega^{\text{tet}}}+\left(\nabla\times\boldsymbol{N}_i^{\text{bse}},\nabla\times\boldsymbol{E}^{\text{bse}}\right)_{\Omega^{\text{bse}}}-\left(\hat{\boldsymbol{n}}\times[\![\boldsymbol{N}_i]\!],\{\!\{\nabla\times\boldsymbol{E}\}\!\}_\alpha\right)_\Gamma-\left(\{\!\{\nabla\times\boldsymbol{N}_i\}\!\}_\alpha,\hat{\boldsymbol{n}}\times[\![\boldsymbol{E}]\!]\right)_\Gamma\\&+\gamma\left(\hat{\boldsymbol{n}}\times[\![\boldsymbol{N}_i]\!],h^{-1}\hat{\boldsymbol{n}}\times[\![\boldsymbol{E}]\!]\right)_\Gamma\\&=\mu_0\epsilon_0\omega^2\left[\left(\boldsymbol{N}_i^{\text{tet}},\epsilon_{\text{r}}\boldsymbol{E}^{\text{tet}}\right)_{\Omega^{\text{tet}}}+\left(\boldsymbol{N}_i^{\text{bse}},\epsilon_{\text{r}}\boldsymbol{E}^{\text{bse}}\right)_{\Omega^{\text{bse}}}\right].\end{aligned} \tag{5}$$

The solution of Maxwell's equations (1)–(4) satisfies the weak formulation (5), which makes the weak formulation consistent with the original problem in that sense. The term $\left(\hat{\boldsymbol{n}}\times[\![\boldsymbol{N}_i]\!],\{\!\{\nabla\times\boldsymbol{E}\}\!\}_\alpha\right)_\Gamma$ is a result of integration by parts of the curl–curl operator given that the electric field features a discontinuous tangential component at the interface Γ. Finally, the additional term $\left(\{\!\{\nabla\times\boldsymbol{N}_i\}\!\}_\alpha,\hat{\boldsymbol{n}}\times[\![\boldsymbol{E}]\!]\right)_\Gamma$ yields symmetry and the remaining term $\gamma\left(\hat{\boldsymbol{n}}\times[\![\boldsymbol{N}_i]\!],h^{-1}\hat{\boldsymbol{n}}\times[\![\boldsymbol{E}]\!]\right)_\Gamma$ makes it possible to stabilize the stiffness matrix, where the so-called stabilization parameter $\gamma\geq 0$ can be chosen. The weighted average of $\boldsymbol{E}$ at the interface Γ is denoted $\{\!\{\boldsymbol{E}\}\!\}_\alpha=\alpha\boldsymbol{E}^{\text{bse}}+(1-\alpha)\boldsymbol{E}^{\text{tet}}$, where we can choose the weight $\alpha\in[0,1]$.

The weak form is expressed as a system of linear equations

$$\left(\mathbf{S}-\mathbf{S}^{\Gamma}+\gamma\mathbf{S}^{\Gamma_{\text{s}}}\right)\mathbf{e}=\mu_0\epsilon_0\omega^2\mathbf{M}\mathbf{e}, \tag{6}$$

where the elements in the stiffness and mass matrices are given by

$$\begin{aligned}S_{i,j}&=\left(\nabla\times\boldsymbol{N}_i^{\text{tet}},\nabla\times\boldsymbol{N}_j^{\text{tet}}\right)_{\Omega^{\text{tet}}}+\left(\nabla\times\boldsymbol{N}_i^{\text{bse}},\nabla\times\boldsymbol{N}_j^{\text{bse}}\right)_{\Omega^{\text{bse}}}\\S_{i,j}^{\Gamma}&=\left(\hat{\boldsymbol{n}}\times[\![\boldsymbol{N}_i]\!],\{\!\{\nabla\times\boldsymbol{N}_j\}\!\}_\alpha\right)_\Gamma+\left(\{\!\{\nabla\times\boldsymbol{N}_i\}\!\}_\alpha,\hat{\boldsymbol{n}}\times[\![\boldsymbol{N}_j]\!]\right)_\Gamma\\S_{i,j}^{\Gamma_{\text{s}}}&=\left(\hat{\boldsymbol{n}}\times[\![\boldsymbol{N}_i]\!],h^{-1}\hat{\boldsymbol{n}}\times[\![\boldsymbol{N}_j]\!]\right)_\Gamma\\M_{i,j}&=\left(\boldsymbol{N}_i^{\text{tet}},\epsilon_{\text{r}}\boldsymbol{N}_j^{\text{tet}}\right)_{\Omega^{\text{tet}}}+\left(\boldsymbol{N}_i^{\text{bse}},\epsilon_{\text{r}}\boldsymbol{N}_j^{\text{bse}}\right)_{\Omega^{\text{bse}}}\end{aligned}$$

2.2.1. Higher-order basis functions on brick-shaped elements

For the brick-shaped elements in the region Ω^{bse}, the electric field is represented according to $\boldsymbol{E}^{\text{bse}}=\sum_j e_j^{\text{bse}}\boldsymbol{N}_j^{\text{bse}}$. Given this situation, it is desirable and possible to construct a diagonal mass-matrix, which is attractive since it allows for explicit time-stepping. (It should be noted that curl-conforming basis functions on brick-shaped elements have a constant direction that is parallel to one of the Cartesian axes of the element and, thus, perpendicular to the other Cartesian axes of the element. As a consequence, the orthogonality of the basis functions' vector field yields a block-diagonal mass-matrix.) In order to achieve a diagonal mass-matrix, we use the construction presented by Cohen [3], which is based on interpolatory polynomials as basis functions. To achieve mass-lumping, the interpolation points of the basis functions are collocated with the quadrature points of appropriately chosen quadrature schemes of sufficiently high accuracy.

In particular, the curl-conforming basis $\boldsymbol{N}_j$ of incomplete order p is constructed on the reference hexahedron ($0 \le u \le 1$, $0 \le v \le 1$ and $0 \le w \le 1$) as

$$\boldsymbol{N}^u_{lmn} = \hat{\boldsymbol{u}}\, G_l(u) L_m(v) L_n(w) \tag{7}$$

$$\boldsymbol{N}^v_{lmn} = \hat{\boldsymbol{v}}\, L_l(u) G_m(v) L_n(w) \tag{8}$$

$$\boldsymbol{N}^w_{lmn} = \hat{\boldsymbol{w}}\, L_l(u) L_m(v) G_n(w) \tag{9}$$

Here, we use the set of polynomials $\mathbb{L} = \{L_l(u)\}_{l=1}^{p+1}$ that have interpolation points that coincide with the quadrature points $0 = \xi^{\mathrm{L}}_1 < \xi^{\mathrm{L}}_2 < \ldots < \xi^{\mathrm{L}}_{p+1} = 1$ of the Gauss–Lobatto rule for the interval $[0, 1]$, such that $L_l(\xi^{\mathrm{L}}_m) = \delta_{lm}\ \forall\ l, m$. Similarly, we use the set of polynomials $\mathbb{G} = \{G_l(u)\}_{l=1}^{p}$ with interpolation points that coincide with the quadrature points $\{\xi^{\mathrm{G}}_l\}_{l=1}^{p}$ of the Gauss rule for the same interval $[0, 1]$, such that $G_l(\xi^{\mathrm{G}}_m) = \delta_{lm}\ \forall\ l, m$.

2.2.2. Higher-order basis functions on tetrahedrons

For the tetrahedral elements in the region Ω^{tet}, the electric field is represented according to $\boldsymbol{E}^{\mathrm{tet}} = \sum_j e^{\mathrm{tet}}_j \boldsymbol{N}^{\mathrm{tet}}_j$. For this region, we use the hierarchical basis functions of incomplete or complete order p presented by Ingelström [10]. The hierarchical basis functions are a particular variation of the set of basis functions defined by Webb [16] and they are constructed such that the basis functions of order $q > p$ vanish when they are projected onto the $\mathcal{H}(\mathbf{curl}, \Omega)$ conforming (Nédélec) FE space $\mathcal{W}_p$ by the Nédélec interpolation operator $\boldsymbol{\pi}^p$ [5]. This feature makes the basis well-suited for the use with efficient multilevel solvers and goal-oriented hierarchical error estimators. Moreover, the hierarchical basis functions are suitable for *hp*-refinement schemes.

2.3. Tangential continuity at the hybrid interface

Given the curl-conforming elements on the brick-shaped elements and the tetrahedrons, there are two different expansions of the electric field at the interface Γ: (i) the representation of $\boldsymbol{E}^{\mathrm{tet}} = \sum_j e^{\mathrm{tet}}_j \boldsymbol{N}^{\mathrm{tet}}_j$ as the interface Γ is approached from the region Ω^{tet}; and (ii) the representation of $\boldsymbol{E}^{\mathrm{bse}} = \sum_j e^{\mathrm{bse}}_j \boldsymbol{N}^{\mathrm{bse}}_j$ as the interface Γ is approached from the region Ω^{bse}.

2.3.1. Lowest-order hybrid

The lowest-order curl-conforming basis is denoted by $p = 1_{\mathrm{i}}$, where the subindex "i" indicates that the basis is *incomplete* linear (i.e. the field components are not linear in all space coordinates). For the lowest-order basis functions, it is not possible to achieve pointwise tangential continuity at the interface between brick-shaped elements ($p^{\mathrm{bse}} = 1_{\mathrm{i}}$) and tetrahedrons ($p^{\mathrm{tet}} = 1_{\mathrm{i}}$). However, Degerfeldt et al. [9] found that the tetrahedral degrees of freedom at the interface can be eliminated such that the resulting method works well: (i) no spurious solution; (ii) quadratic convergence for regular problems; (iii) low reflection-coefficient at the hybrid interface; and (iv) stable hybrid explicit–implicit time-stepping. With reference to Fig. 1, the procedure is straight-forward for the edges j that coincide at the interface, where the relation is $e^{\mathrm{tet}}_j = e^{\mathrm{bse}}_j$ for a rectangular face with constant w-coordinate and edges $j = u_1, u_2, v_1$ and v_2. For the tetrahedral edge d that coincides with the diagonal of the rectangular face of the brick-shaped element, the corresponding relation is

$$e^{\mathrm{tet}}_d = \frac{l_{\mathrm{u}}}{l_{\mathrm{d}}} \frac{e^{\mathrm{bse}}_{u_1} + e^{\mathrm{bse}}_{u_2}}{2} + \frac{l_{\mathrm{v}}}{l_{\mathrm{d}}} \frac{e^{\mathrm{bse}}_{v_1} + e^{\mathrm{bse}}_{v_2}}{2}, \tag{10}$$

where l_{u} and l_{v} denote the length of the edges parallel to the u- and v-axis. Similarly, $l_{\mathrm{d}} = \sqrt{l^2_{\mathrm{u}} + l^2_{\mathrm{v}}}$ is the length of the diagonal of the rectangular face. In Eq. (6), this construction yields $\mathbf{S}^{\Gamma} = \mathbf{0}$ and, thus, stabilization is not needed, which makes it possible to set $\gamma = 0$. It should be emphasized that this construction with $p^{\mathrm{bse}} = p^{\mathrm{tet}} = 1_{\mathrm{i}}$ is attractive since the incomplete-order basis functions keep the number of degrees of freedom per element at a minimum.

2.3.2. Hybrids with incomplete bricks and complete tetrahedrons

Another option is to use an incomplete-order basis on the brick-shaped elements in combination with the corresponding complete-order (subindex "c") basis on the tetrahedrons, such that $(p^{\mathrm{bse}}, p^{\mathrm{tet}}) = (1_{\mathrm{i}}, 1_{\mathrm{c}}), (2_{\mathrm{i}}, 2_{\mathrm{c}}), (3_{\mathrm{i}}, 3_{\mathrm{c}})$, etc. Then, it is straight-forward to enforce pointwise tangential continuity in the strong sense by means of (i) the projection of the basis of the brick-shaped elements onto the tetrahedral degrees of freedom [10] or (ii) fitting by Galerkin's method such that the tangential field is continuous [11,12]. However, a tetrahedral mesh with $p^{\mathrm{tet}} = 1_{\mathrm{c}}, 2_{\mathrm{c}}, 3_{\mathrm{c}}, \ldots$ yields more degrees of freedom as compared to $p^{\mathrm{tet}} = 1_{\mathrm{i}}, 2_{\mathrm{i}}, 3_{\mathrm{i}}, \ldots$ and, in addition, the extra degrees of freedom needed for the complete-order approximation of the field do not contribute to the modeling of its curl.

2.3.3. Higher-order hybrids with Nitsche's method

For higher-order hybrid methods with $p^{\mathrm{bse}} = p^{\mathrm{tet}} = 2_{\mathrm{i}}, 3_{\mathrm{i}}, \ldots$, we use our weak formulation (5) to enforce tangential continuity at the interface Γ in the weak sense, which gives an efficient method that works well and preserves the advantageous properties of the lowest-order method [9]. However, the higher-order hybrid yields $\mathbf{S}^{\Gamma} \neq \mathbf{0}$ and requires stabilization by $\gamma > 0$.

2.3.4. Additional remarks

Thus, it is desirable to use incomplete-order basis functions on the tetrahedrons and, only if decided by the user, employ complete-order basis functions. It should be emphasized that our weak formulation (5) can handle both cases correctly, which makes it very flexible. However, the lowest-order case $p^{\text{bse}} = p^{\text{tet}} = 1_{\text{i}}$ can not be treated in the weak sense and must be handled by the construction presented by Degerfeldt et al. [9].

2.4. Hybrid explicit–implicit time-stepping scheme

For time-stepping, we exploit a hybrid explicit–implicit time-stepping scheme [8] that is based on a partitioning of the stiffness and mass matrices in terms of contributions from the different elements indexed by k, such that $\mathbf{S} = \sum_k \mathbf{S}_k$ and $\mathbf{M} = \sum_k \mathbf{M}_k$. An implicitness parameter θ_k is associated with each element k and we have the time-stepping scheme

$$\sum_{k=1}^{K} \left(\mathbf{S}_k \left[\theta_k \mathbf{e}^{(n+1)} + (1 - 2\theta_k)\, \mathbf{e}^{(n)} + \theta_k \mathbf{e}^{(n-1)} \right] + \frac{1}{(c_0 \Delta t)^2} \mathbf{M}_k \left[\mathbf{e}^{(n+1)} - 2\mathbf{e}^{(n)} + \mathbf{e}^{(n-1)} \right] \right) = \mathbf{0}, \tag{11}$$

where the time step n is indicated by the superindex such that $\mathbf{e}^{(n)} = \mathbf{e}(t)|_{t=n\Delta t}$. The error of the time-stepping scheme (11) is proportional to Δt^2.

In the context of the hybrid formulation (5), we distinguish between two different types of contributions to the stiffness matrix: (i) volume contributions from the brick-shaped elements in Ω^{bse} are explicitly time-stepped by $\theta_k = 0$; and (ii) volume contributions from the tetrahedrons in Ω^{tet} and surface contributions from the hybrid interface Γ are implicitly time-stepped with $\theta_k \geq 1/4$.

This yields a global time-stepping scheme with a time step that must satisfy a Courant condition $c_0 \Delta t \leq 2/\sqrt{\lambda_{\max}}$ for stability on the brick-shaped elements, where $\lambda_{\max}$ is the largest eigenvalue for the problem $\mathbf{S}_k \mathbf{e} = \lambda \mathbf{M}_k \mathbf{e}$ that is associated with the brick-shaped element k. For a cube of side h, we have $\lambda_{\max} = 12/h^2$ for $p = 1_{\text{i}}$, $\lambda_{\max} = 72/h^2$ for $p = 2_{\text{i}}$, $\lambda_{\max} \lesssim 222.94/h^2$ for $p = 3_{\text{i}}$ and $\lambda_{\max} \lesssim 550.05/h^2$ for $p = 4_{\text{i}}$. The tetrahedrons in Ω^{tet} together with the hybrid interface Γ are implicitly time-stepped with a common value for $\theta_k \geq 1/4$ and stability is achieved for sufficiently large values of the stabilization parameter γ.

3. Results

In this section, we test the hybrid formulation on closed cavity resonators: (i) compute all the eigenvalues by solving the generalized eigenvalue problem (6); and (ii) transform the eigenvalue problem (6) to the time domain and compute the time-domain response given an initial condition, where the spectrum is computed by means of the discrete Fourier transform [17]. In addition, we investigate the reflection coefficient of a layer of tetrahedrons embedded in a structured grid of brick-shaped elements that discretizes a rectangular waveguide, where we solve a driven problem in the frequency domain. In all tests that follow, we use $\alpha = 1$, which gives $\{\!\{\boldsymbol{E}\}\!\}_{\alpha=1} = \boldsymbol{E}^{\text{bse}}$. (For discontinuous Galerkin methods [18,19], it is common to use $\alpha = 1/2$.)

3.1. Canonical cavity resonator as an eigenvalue problem

As a first test problem, we consider a cavity resonator of size 0.9 m × 1.0 m × 1.1 m, where the outer boundary $\partial\Omega$ is a perfect electric conductor and the interior of the cavity is characterized by the permittivity ϵ_0 and the permeability μ_0. The eigenvalues can be calculated analytically for this problem [20], which makes it a useful test case for validation purposes. The cavity resonator is discretized by a hybrid mesh as shown in Fig. 2, where this mesh is uniformly and hierarchically refined for the convergence studies that follow.

We compute the eigenvalue spectrum from Eq. (6), where we use $\gamma = 10^5$ to enforce tangential continuity in the weak sense. All eigenvalues are computed by a direct eigenvalue solver. We find that the lowest non-zero eigenvalues are reproduced with the correct multiplicity and the corresponding eigenfrequencies are presented in Fig. 3. In Fig. 3, the results for the lowest-order hybrid [9] with $p^{\text{bse}} = p^{\text{tet}} = 1_{\text{i}}$ and $\gamma = 0$ are included for comparison, where only five non-zero eigenvalues are available due to the coarse discretization of the cavity resonator shown in Fig. 2. It should be noted that the spectrum contains a large number of zero eigenvalues that correspond to electrostatic modes, where the electric field can be expressed as the gradient of a scalar potential.

Fig. 4 shows the relative error $|f - f_{\text{a}}|/f_{\text{a}}$ for the lowest non-zero eigenfrequency f (with the corresponding exact result f_{a}) as a function of the number of points per wavelength λ/h, where we employ uniform and hierarchical mesh refinement to vary the cell size h. We notice that our hybrid method gives a relative error that is approximately proportional to h^{2p}, which is the order of convergence that is expected for a regular problem solved by elements of polynomial order p.

3.2. Rectangular waveguide in frequency domain

It is desirable to quantify the reflection by a layer of tetrahedrons embedded in a structured grid of brick-shaped elements. Clearly, such a reflection should be small enough in comparison to the corresponding reflection coefficient of the

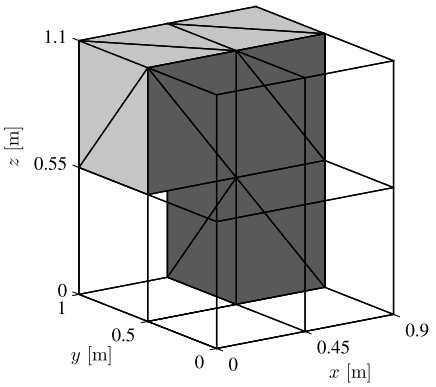

Fig. 2. Geometry for a cavity resonator of size 0.9 m × 1.0 m × 1.1 m, where the outer boundary $\partial\Omega$ is a perfect electric conductor: dark gray triangles – tetrahedral faces that coincide with the hybrid interface Γ; light gray triangles – tetrahedral faces that coincide with the outer boundary $\partial\Omega$; and transparent wire-frame elements – brick-shaped elements in Ω^{bse}.

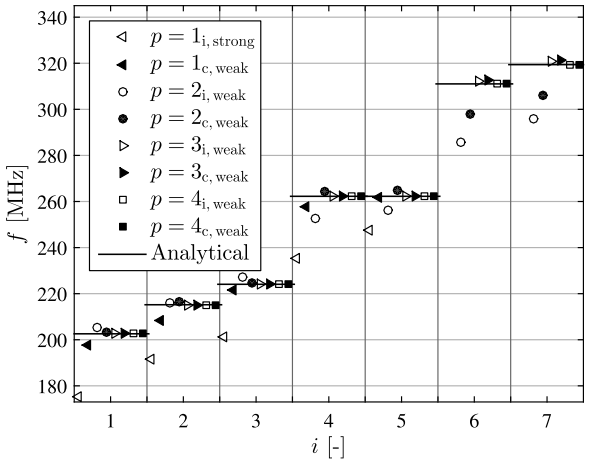

Fig. 3. Spectrum for the lowest non-zero eigenvalues: horizontal solid lines – analytical result; hollow glyphs – incomplete-order basis $p^{\text{bse}} = p^{\text{tet}} = p$; and solid glyphs – complete-order basis $p^{\text{tet}} = p$ for the tetrahedrons and the corresponding incomplete-order basis p^{bse} for the brick-shaped elements. Here, we have linear elements (triangles pointing to the left), quadratic elements (circles), cubic elements (triangles pointing to the right) and quartic elements (squares).

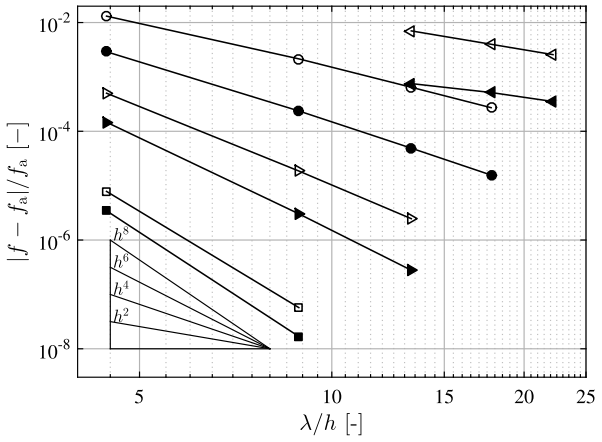

Fig. 4. Relative error for the lowest non-zero eigenvalue: hollow glyphs – incomplete-order basis $p^{\text{bse}} = p^{\text{tet}} = p$; and solid glyphs – complete-order basis $p^{\text{tet}} = p$ for the tetrahedrons and the corresponding incomplete-order basis p^{bse} for the brick-shaped elements. Here, we have linear elements (triangles pointing to the left), quadratic elements (circles), cubic elements (triangles pointing to the right) and quartic elements (squares).

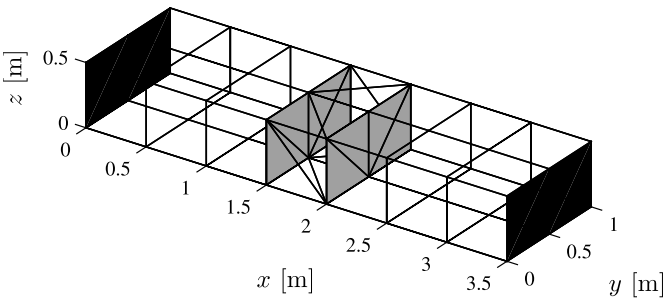

Fig. 5. Rectangular waveguide discretized by a hybrid mesh: light gray triangles – hybrid interface Γ that separates a layer of tetrahedrons Ω^{tet} from the remaining part Ω^{bse} of the waveguide discretized by brick-shaped elements; and dark gray rectangular faces – waveguide ports with Robin boundary conditions.

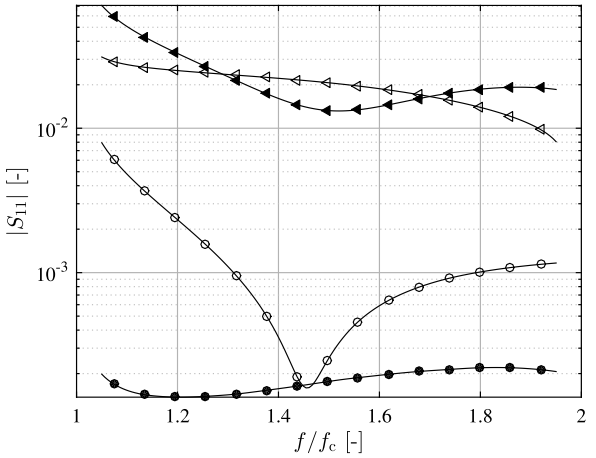

Fig. 6. Reflection coefficient for a layer of tetrahedrons: hollow glyphs – incomplete-order basis $p^{\text{bse}} = p^{\text{tet}} = p$; and solid glyphs – complete-order basis $p^{\text{tet}} = p$ for the tetrahedrons and the corresponding incomplete-order basis p^{bse} for the brick-shaped elements. Here, we have linear elements (triangles) and quadratic elements (circles).

physical phenomena that are subject to investigation. In order to study this aspect of the hybrid method, we discretize a rectangular waveguide of size 3.5 m $\times$ 1.0 m $\times$ 0.5 m by brick-shaped elements, as shown in Fig. 5. For the region 1.5 m $\leq x \leq$ 2.0 m, we sub-divide the brick-shaped elements into tetrahedrons to allow for a study of the reflection coefficient from the layer of tetrahedrons. The hybrid mesh with (typical) cell size h_0 is shown in Fig. 5, where the light gray triangles show the hybrid interface Γ.

The dark gray rectangular faces in Fig. 5 indicate the waveguide ports $r = 1$ and 2 that occupy the surfaces $\partial\Omega_r$, which are part of the outer boundary $\partial\Omega$. At the waveguide ports, we impose the Robin boundary condition

$$\hat{\boldsymbol{n}} \times \nabla \times \boldsymbol{E} + jk_x \hat{\boldsymbol{n}} \times \hat{\boldsymbol{n}} \times \boldsymbol{E} = 2jk_x \hat{\boldsymbol{n}} \times \hat{\boldsymbol{n}} \times \boldsymbol{E}^{\text{inc}}, \tag{12}$$

where $\boldsymbol{E}^{\text{inc}} = \hat{\boldsymbol{z}} E_0^{\text{inc}} \sin(\pi y/a) \exp(jk_x \hat{\boldsymbol{n}} \cdot \boldsymbol{r})$ is the incident field of the fundamental waveguide-mode (TE_{10}-mode) of the rectangular waveguide [20] and $a = 1.0$ m is the width of the waveguide. The remaining part of the outer boundary $\partial\Omega$ is modeled as a perfect electric conductor. The analytical wavenumber is given by $k_x = \sqrt{(\omega/c_0)^2 - (\pi/a)^2}$. For the tests that follow, we tune the wavenumber $k_x = k_x(\omega)$ used in the boundary condition (12) for a waveguide discretized by *only* brick-shaped elements such that the reflection coefficient is minimized for each frequency ω, which makes undesired reflections at the waveguide ports negligible as compared to the reflection from the layer of tetrahedrons.

The mesh in Fig. 5 with cell size h_0 is hierarchically refined such that $h = h_0/4$ and we use linear and quadratic basis functions to compute the reflection coefficient from the layer of tetrahedrons. The computed reflection coefficient is shown in Fig. 6 as a function of the normalized frequency f/f_c, where f_c is the cutoff frequency for the TE_{10}-mode.

Next, we perform the same test for cubic and quartic basis functions. Since the number of degrees of freedom per element increases dramatically with the polynomial order, we use the mesh shown in Fig. 5 with cell size h_0 directly without any mesh refinements. The reflection coefficient is shown in Fig. 7 as a function of f/f_c and it is clear that the reflection coefficient is significantly reduced by the higher-order basis functions despite the fact that the elements are considerably larger in size as compared to the discretization used in Fig. 6.

Next, we compute the average $|S_{11}|_{\text{avg}}$ of the reflection coefficient's magnitude, where the average is evaluated for the frequency band $1.05 \leq f/f_c \leq 1.95$. Fig. 8 shows the averaged reflection coefficient $|S_{11}|_{\text{avg}}$ as a function of the number of

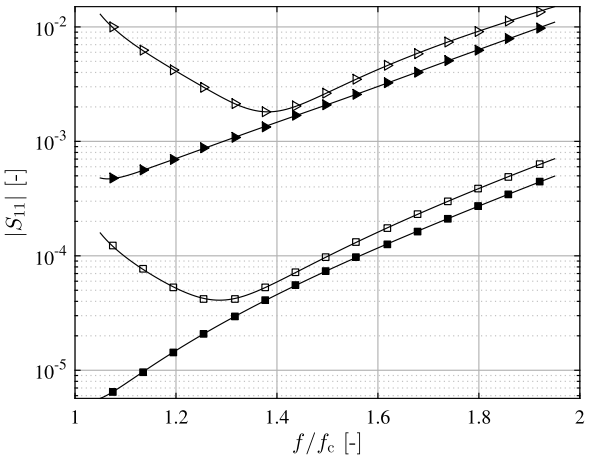

Fig. 7. Reflection coefficient for a layer of tetrahedrons: hollow glyphs – incomplete-order basis $p^{\text{bse}} = p^{\text{tet}} = p$; and solid glyphs – complete-order basis $p^{\text{tet}} = p$ for the tetrahedrons and the corresponding incomplete-order basis p^{bse} for the brick-shaped elements. Here, we have cubic elements (triangles) and quartic elements (squares).

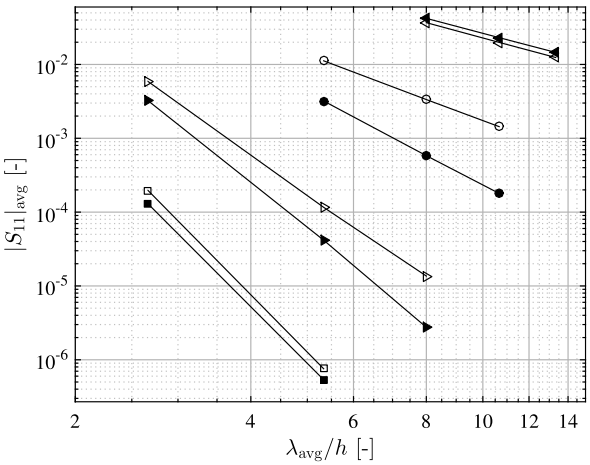

Fig. 8. Reflection coefficient for a layer of tetrahedrons of fixed thickness as a function of the cell size: hollow glyphs – incomplete-order basis $p^{\text{bse}} = p^{\text{tet}} = p$; and solid glyphs – complete-order basis $p^{\text{tet}} = p$ for the tetrahedrons and the corresponding incomplete-order basis p^{bse} for the brick-shaped elements. Here, we have linear elements (triangles pointing to the left), quadratic elements (circles), cubic elements (triangles pointing to the right) and quartic elements (squares).

cells per wavelength λ_{avg}/h, where λ_{avg} is the wavelength that corresponds to the frequency $f = 1.5 f_c$ and the cell size h is reduced by means of hierarchical mesh-refinement. It is found that the higher-order hybrid method yields a significantly reduced reflection coefficient as the order of the basis is increased and that the reflection coefficient scales approximately as h^{2p}.

3.3. Cavity resonator in time domain

The final test case is the cavity resonator shown in Fig. 9, which is based on a brick-shaped cavity resonator with two edges of the cavity cut away and replaced by 45°-chamfers. The regions around these chamfers are discretized by tetrahedrons: dark gray triangles – tetrahedral faces that coincide with the hybrid interface Γ; light gray triangles – tetrahedral faces that coincide with the outer boundary $\partial\Omega$ of the cavity resonator. The outer boundary $\partial\Omega$ is modeled as a perfect electric conductor.

Given the hybrid method with $p^{\text{bse}} = p^{\text{tet}} = 3_{\text{i}}$ and $\gamma = 10^5$, we solve for the electric field in the time-domain by the hybrid explicit–implicit time-stepping scheme (11), where we initialize the two first solution vectors $\mathbf{e}^{(-1)} = \mathbf{e}^{(0)}$ by random numbers and employ the implicitness parameter $\theta_k = 1/4$ for all terms k that are not associated with the brick-shaped elements. The time-stepping algorithm was executed for 300,000 time-steps and we note that the numerical solution does not show any signs of instability. Some arbitrarily chosen elements in $\mathbf{e}^{(n)}$ are added to give the signal $s^{(n)}$ and its discrete Fourier transform [17] is shown in Fig. 10 as a solid curve. In addition, we computed the eigenfrequencies by a standard curl-conforming FEM implemented in the commercial package `COMSOL multiphysics` [21] and

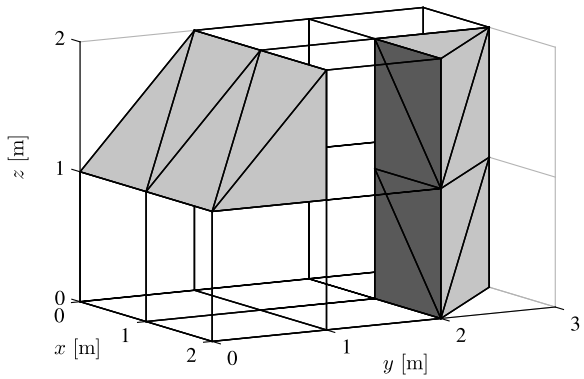

Fig. 9. Geometry for a cavity resonator where the outer boundary $\partial\Omega$ is a perfect electric conductor: dark gray triangles – tetrahedral faces that coincide with the hybrid interface Γ; light gray triangles – tetrahedral faces that coincide with the outer boundary $\partial\Omega$; and transparent wire-frame elements – brick-shaped elements in Ω^{bse}.

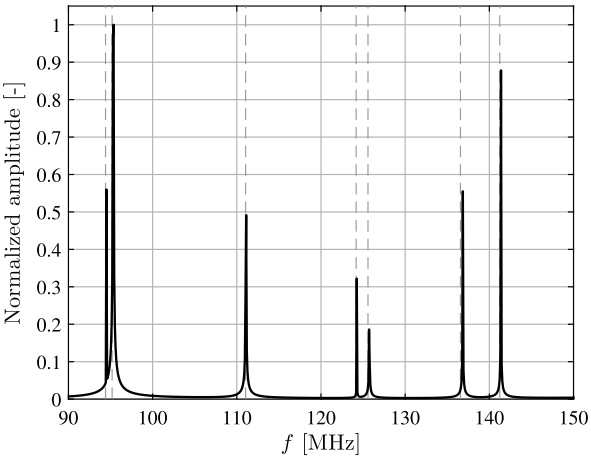

Fig. 10. Spectrum for the cavity resonator shown in Fig. 9: solid curve – discrete Fourier transform of the electric field sampled at a number of points inside the cavity resonator for a duration of 300,000 time steps; and dashed vertical lines – eigenfrequencies computed by `COMSOL multiphysics`.

the results are shown as dashed vertical lines in Fig. 10. We note that the peaks in the spectrum computed by means of the hybrid method (5) in time domain agree well with the eigenfrequencies computed by means of `COMSOL multiphysics`.

4. Conclusion

We present a finite element method (FEM) for Maxwell's equations that combines (i) a grid of structured brick-shaped elements for large homogeneous regions with (ii) a mesh of unstructured tetrahedrons for regions that feature complex geometry or rapid field variations. The two discretizations are non-overlapping and they share the common interface Γ, where the tangential component of the electric field may be discontinuous. Tangential continuity is enforced in the weak sense by means of Nitsche's method and the weak form features a stabilization parameter that can be chosen. The hybrid method preserves the null-space of the curl-operator and reproduces the lowest non-zero eigenvalues of cavity resonators with the correct multiplicity, where the numerical solution converges towards the analytical result with an error that is approximately proportional to h^{2p} for cavities without reentrant corners or edges. Here, the cell size is denoted h and the polynomial order of the element is denoted p. A layer of tetrahedrons embedded in a waveguide discretized by brick-shaped elements yields a low reflection-coefficient that scales approximately as h^{2p}.

For transient field-problems, we use a second-order accurate hybrid explicit–implicit time-stepping scheme with an implicitness parameter θ_k associated with the elements indexed by k. Explicit time-stepping for the mass-lumped brick-shaped elements is achieved by choosing $\theta_k = 0$, which yields a standard Courant condition on the global time-step. For the unstructured tetrahedrons and the terms in the weak form that are associated with the hybrid interface Γ, we use $\theta_k \geq 1/4$ and, for a sufficiently large value of the stabilization parameter γ, this yields unconditionally stable time-stepping.

Acknowledgements

This work was supported in part by the Swedish Research Council (dnr 2010–4627) in the project "Model-based Reconstruction and Classification Based on Near-Field Microwave Measurements". The computations were performed on resources at Chalmers Centre for Computational Science and Engineering (C3SE) provided by the Swedish National Infrastructure for Computing (SNIC).

References

[1] K.S. Yee, Numerical solution of initial boundary value problems involving Maxwell's equations in isotropic media, IEEE Trans. Antennas Propag. AP-14 (3) (1966) 302–307.
[2] A. Taflove, S.C. Hagness, Computational Electrodynamics: The Finite-Difference Time-Domain Method, 3rd edition, Artech House, Boston, MA, 2005.
[3] G. Cohen, Higher Order Numerical Methods for Transient Wave Equations, Springer, Berlin, 2002.
[4] J.M. Jin, The Finite Element Method in Electromagnetics, 2nd edition, John Wiley & Sons, New York, NY, 2002.
[5] J.C. Nédélec, Mixed finite elements in $\mathbb{R}^3$, Numer. Math. 35 (3) (1980) 315–341.
[6] G. Cohen, P. Monk, Gauss point mass lumping schemes for Maxwell's equations, Numer. Methods Partial Differ. Equ. 14 (1) (1998) 63–88.
[7] M.L. Stowell, B.J. Fasenfest, D.A. White, Investigation of radar propagation in buildings: a 10-billion element Cartesian-mesh FETD simulation, IEEE Trans. Antennas Propag. 56 (2008) 2241–2250.
[8] T. Rylander, A. Bondeson, Stability of explicit–implicit hybrid time-stepping schemes for Maxwell's equations, J. Comput. Phys. 179 (2002) 426–438.
[9] D. Degerfeldt, T. Rylander, A brick-tetrahedron finite-element interface with stable hybrid explicit–implicit time-stepping for Maxwell's equations, J. Comput. Phys. 220 (2006) 383–393.
[10] P. Ingelström, A new set of $\boldsymbol{H}$(curl)-conforming hierarchical basis functions for tetrahedral meshes, IEEE Trans. Microw. Theory Tech. 54 (1) (2006) 106–114.
[11] N. Marais, D.B. Davidsson, Conforming arbitrary order hexahedral/tetrahedral hybrid discretisation, Electron. Lett. 44 (24) (2008) 1384–1385.
[12] N. Marais, D.B. Davidsson, Efficient high-order time domain hybrid implicit/explicit finite element methods for microwave electromagnetics, Electromagnetics 30 (1–2) (2010) 127–148.
[13] P. Hansbo, Nitsche's method for interface problems in computational mechanics, GAMM-Mitt. 28 (2) (2005) 184–207.
[14] F. Assous, M. Michaeli, Solving Maxwell's equations in singular domains with a Nitsche type method, J. Comput. Phys. 230 (2011) 4922–4939.
[15] A. Taflove, Advances in Computational Electrodynamics: The Finite-Difference Time-Domain Method, Artech House, Boston, MA, 1998.
[16] J.P. Webb, Hierarchal vector basis functions of arbitrary order for triangular and tetrahedral finite elements, IEEE Trans. Antennas Propag. 47 (8) (1999) 1244–1253.
[17] W.H. Press, S.A. Teukolsky, W.T. Vetterling, B.P. Flannery, Numerical Recipes in C: The Art of Scientific Computing, 2nd edition, Cambridge University Press, New York, NY, 1992.
[18] P. Houston, I. Perugia, A. Schneebeli, D. Schötzau, Interior penalty method for the indefinite time-harmonic Maxwell equations, Numer. Math. 100 (2005) 485–518.
[19] T. Warburton, M. Embree, The role of the penalty in the local discontinuous Galerkin method for Maxwell's eigenvalue problem, Comput. Methods Appl. Mech. Eng. 195 (2006) 3205–3223.
[20] C.A. Balanis, Advanced Engineering Electromagnetics, John Wiley & Sons, New York, NY, 1989.
[21] Comsol multiphysics, http://www.comsol.com.